Erschienen in: Polymer. Elsevier. 2023, 282, 126181
https://doi.org/10.1016/j.polymer.2023.126181

Effect of CH_2 run length on the crystallization kinetics of sustainable long-spaced aliphatic polyesters

Stephanie F. Marxsen [a], Manuel Häußler [b], Marcel Eck [b], Stefan Mecking [b], Rufina G. Alamo [a,*]

[a] *FAMU-FSU College of Engineering, Department of Chemical and Biomedical Engineering, 2525 Pottsdamer St, Tallahassee, FL, 32310, USA*
[b] *Department of Chemistry, University of Konstanz, Universitätsstraße 10, 78457, Konstanz, Germany*

Keywords:
Aliphatic polyesters
Symmetric aliphatic polyesters
Long-spaced
Crystallization kinetics
Self-poisoning
Polyethylene-like materials

A B S T R A C T

We have studied the isothermal overall crystallization rates and linear growth rates of four symmetric long-spaced aliphatic polyesters (LSAPEs) with 12, 18, 32, or 48 carbons in both the diol and the diacid monomers. With increasing crystallization temperature (T_c) these LSAPEs display discrete rate minima in a number and depth that depend on the length of the methylene spacer between esters. Two rate minima are observed for PE-48,48 and for PE-32,32; one for PE-18,18 and none for PE-12,12. The rate minima are not associated with a change in the mechanism of nucleation and growth or with a change in crystal packing, but occur at T_c where the crystal thickness transitions from a non-integer to a quantized integer number of monomer units. We explain such rate minima based on the *self-poisoning* feature used earlier to explain similar findings in *n*-alkanes and other types of precision polyethylene-like systems. In LSAPEs, metastable non-integer crystals attach to the growth front of stable integer crystals retarding their growth until the non-integer segments thicken to complete the layer. Lack of rate minima in the shortest-spaced symmetric polyester is explained by a small difference in lamellar thickness between non-integer and integer layered crystals which favors the formation of integer crystals at any T_c.

1. Introduction

The terminology "long-chain" or "long-spaced" aliphatic polyesters (LSAPE) usually refers to polyesters with ≥14 consecutive methylenes between ester bonds [1]. These polyesters have melting temperatures close to or higher than 100 °C, relatively high levels of crystallinity, and the continuous long methylene sequences confer properties similar to those of many commercial polyethylenes. Moreover, unlike most polyethylenes, the monomers can be obtained from biosources, and the in-chain ester groups can be hydrolyzed in principle, thus adding the possible benefit of either biodegradation, or closed-loop recyclability as recently demonstrated [2,3]. LSAPEs and other types of aliphatic polyesters have been identified as sustainable alternatives to commodity polymers synthesized from fossil fuels. In addition to biodegradable bioplastics produced in large scale, such as polylactic acid, poly (butylene-adipate-co-terephthalate), poly(hydroxy alkanoates) and poly (butylene succinate) [4,5], biodegradable aliphatic polyesters could be used to manufacture products that alleviate the problems associated with discarded plastics made of traditional poorly recyclable and nondegradable polyethylenes [6]. Poly(alkylene dicarboxylate)s have been synthesized via different methods [7–10], reaching up to 48 carbons in the aliphatic sequences of both the diol and the diacid [11].

In parallel with synthetic efforts, the melting behavior and some crystalline properties of mainly short-spaced aliphatic polyesters, have also been analyzed in some detail [12–25]. For a fixed number of carbons in the diol, with increasing carbons in the diacid, the melting temperature first decreases sharply reaching a minimum at 3 carbons, and then increases in a zig-zag pattern between even (higher melting points) and odd (lower melting points) number of carbons [1,26]. The melting point difference between even and odd-spaced ester groups becomes smaller with increasing number of carbons and eventually vanishes for > ~10 carbons between esters, but the melting point continues to increase as the length of the methylene spacer increases approaching the melting temperature of linear polyethylene. The zig-zag melting effect of aliphatic polyesters may originate from ester dipoles in the layered crystalline regions pointing in either the opposite (even carbon numbers), or in the same (odd number of carbons) direction. The result is a cancelation of polarization in the crystal for the even spaced, or an increase in polarization for the odd spaced, which affects crystal stability and the melting behavior of poly(alkylene dicarboxylate)s

* Corresponding author.
E-mail address: alamo@eng.fsu.edu (R.G. Alamo).

accordingly [1,26]. As the number of carbons in the diacid increases, the interchain CH_2 Van der Waals interactions compensate for the polarization effect, and the odd-even effect on melting vanishes.

While the polarization effect may be a contributor of the odd-even effect on polyester melting, the configuration of consecutive ester groups with respect to the even or odd methylene runs also affects the staggering of the ester groups in crystalline layers, and thus must contribute as well to the odd-even effect on melting. An example of the latter is the well-known odd-even effect on melting of n-alkanes [27,28]. While most even spaced polyesters pack in *all-trans* orthorhombic unit cells, the short-spaced polyesters with odd number of carbons (<5 C) pack in monoclinic structures [12,24,25,29–34]. Some of the odd-spaced polyesters pack in orthorhombic structures with kink conformations [24].

The crystalline properties of LSAPEs, those with >10 CH_2 in diol and/or diacid, are less studied. First, the available data for these systems is limited due in part to synthetic difficulties, and because quite often the focus was on rapid biodegradability, which diminishes in the increasingly hydrophobic polyesters with longer CH_2 sequences [35,36]. The study of crystallization kinetics and the crystalline structure that polyesters develop on cooling from the melt is also important in view of possible commercial viability. Most available kinetic studies are for short type aliphatic polyesters [16–21]. Among LSAPEs, crystallization kinetics have been studied in polytridecanolactone (PE-13) and polypentadecanolactone (PE-15) [37,38], as well as in systems derived from 1,9-nonanediol [39].

The isothermal crystallization rates measured by DSC in PE-13 and PE-15 displayed a continuous decrease with increasing crystallization temperature (T_c). The analysis of the rates according to secondary nucleation theory indicated a transition from Regime I to II with increasing undercooling, and slopes in agreement with the theoretical predictions. The spherulitic morphology also changed from axialites to banded spherulites with increasing undercooling [38]. Moreover, regime transitions were not found in the analysis of the spherulitic growth rates of the odd-spaced polyesters PE-9,9 and PE-9,7 [39]. Avrami analysis of the DSC exotherms recorded under isothermal conditions indicated exponents ~3, which are consistent with the expected heterogeneous athermal nucleation and three-dimensional spherulitic growth. All had wide-angle X-ray diffraction patterns equivalent to the orthorhombic packing of polyethylene.

Contrasting the above behavior, the isothermal overall and linear growth rates of polyethylene brassylate, a short-long type of aliphatic polyester PE-2,13, also referred to as PEB, display discrete deep minima at crystallization temperatures where the crystal thickness undergoes a quantized step increase equivalent to the length of a monomer unit [40]. Two rate minima were observed at T_c = 40 °C corresponding to a transition between 2 and 3 repeats, and at T_c = 60 °C when the crystal thickness changes from 3 to 4 monomer repeats. WAXD patterns are conserved in the whole isothermal crystallization range, thus ruling out any thermally-induced polymorphic change at the T_c where the rate minima are observed. Such rate minima observed in PEB are equivalent to the behavior of *n*-alkanes and low-M_w PEO fractions, and were explained by the manifestation of self-poisoning [41–44]. At T_c approaching a rate minimum from above, metastable but kinetically favored non-integer segments attach to the growth front integer thick crystals. Moreover, the metastable segments need to thin or thicken toward the stable structure with an integer number of repeats. Hence, it was perceived that the attached metastable segments extend in the chain axis to complete the more stable integer crystalline layer for growth to proceed. Such rearrangement takes some time and retards crystal growth, as observed [40]. Evidence of the metastability of non-integer crystals of LSAPEs was given in a prior work which demonstrated that non-integer crystals undergo isothermal step-thickening with time toward the integer layered crystal structure [45].

Rate minima were also found in other polyethylene-like materials with either halogens [46,47] or acetal groups [48–50] inserted in polyethylene backbones at equal distances changing between 6 and 26 CH_2. Interestingly, in addition to a possible change in crystal thickness at the rate minima as found in some of the polyacetals [49], we observed a major polymorphic transition at crystallization temperatures corresponding to the rate minima. Furthermore, a deep minimum in heat of fusion is also found in the narrow T_c range of the rate minima, indicating that low levels of crystallinity develop at the transition between different polymorphs or between structures with quantized crystal thicknesses. Clearly, the rate minima are associated with low crystallinity kinetic traps that may be of practical relevance in melt-processing of polyethylene-like materials.

The manifestation of crystallization rate minima is independent of molecular weight, as demonstrated by the same behavior of three PEB samples studied in a range of M_w from 27,000 to 188,000 g/mol [40]. Therefore, the above extended studies point to a general behavior for the crystallization kinetics of precision polyethylene-like materials. The kinetics are characterized by discrete rate minima in a narrow range of crystallization temperatures where the system transitions between two energetically inequivalent crystal structures differing in crystallographic packing or in quantized crystal thicknesses.

In the present manuscript, we continue our studies of crystallization kinetics of polyethylene-like materials by selecting a series of even-spaced symmetric LSAPEs. Data for overall crystallization rates measured by DSC and FSC, and for linear growth rates measured by polarized optical microscopy are discussed for LSAPEs with 48, 32, 18, or 12 carbons in both the diol and the diacid components of their repeating units. With this even-spaced series of LSAPEs we avoid possible odd-even complications and thus analyze more directly the effect of a decreasing number of carbons between esters in the crystalline layered structure, the crystallization kinetics, and in the manifestation of rate minima.

2. Experimental section

2.1. Materials

The LSAPEs studied here were synthesized by A_2 + B_2 polycondensation, with diol and diacid components each containing 12, 18, 32, or 48 carbon atoms, as described previously [2,11]. Molar mass and DSC thermal characterization data recorded at 10 °C min^{-1} are shown in Table 1. Thermograms from which the thermal characterization data were obtained were discussed in prior works [45,51] and together with new data for PE-12,12, are shown in Fig. S1.

2.2. Thermal analysis

Isothermal crystallization experiments were conducted in a TA Q2000 differential scanning calorimeter (DSC) connected to an RC900 intracooler to allow for subambient temperature control. Static temperature, thermal lag, and heat of fusion were calibrated with indium, and operation occurred under dry N_2 flow. The onset of the exotherm recorded by cooling from the melt at 10 °C min^{-1} was used as a low temperature limit for the isothermal temperature range studied. To capture exotherms during isothermal crystallization, samples were first brought to 150 °C (or > 30 °C above the observed melting peak), held for 5 min to erase thermal history, and then cooled at a rate of 40 °C min^{-1} to the isothermal crystallization temperature, T_c. After holding at T_c for long enough to capture the full exotherm, or another predetermined crystallization time, samples were heated from the T_c at 10 °C min^{-1} to observe the melting endotherm. The overall crystallization rate was associated with the inverse of the peak time of the crystallization exotherm, ($t_{0.5}^{-1}$).

Fast scanning calorimetry (FSC) was used to extend the isothermal crystallization range to higher undercooling than available via classical DSC. We used a Mettler Toledo Flash DSC 1 connected to a Huber TC100 intracooler and operated under dry N_2 flow. FSC sensors were

Table 1
Molar mass and thermal characterization of long-spaced aliphatic polyesters.

Sample	Ester groups per 100 CH_2	M_w [kg mol ^{1}]	M_w M_n ^{1}	$T_{c\ peak}$[°C] [d]	$T_{m\ peak}$[°C] [d]	ΔH_m[J g ^{1}] [d]
PE-48,48	2.1	26 [a]	1.9	108.8	117.8	180
PE-32,32	3.2	77 [a]	2.5	99.8	110.9	160
PE-18,18	5.9	90 [b]	1.9	85.6	97.8	143
PE-12,12	9.1	80 [c]	2.5	71.2	83.9	126

[a] Determined by GPC at 160 °C in 1,2,4-trichlorobenzene against polyethylene standards.
[b] Determined by GPC at 160 °C in 1,2-dichlorobenzene against polystyrene standards.
[c] Determined by GPC at 35 °C in chloroform against polystyrene standards.
[d] Highest crystallization peak ($T_{c\ peak}$), highest melting peak ($T_{m\ peak}$), and observed total heat of fusion (ΔH_m) obtained by DSC at 10 °C min^{-1}.

conditioned and temperature corrected according to manufacturer specifications prior to loading ~40 *n*g of the sample. The temperature correction was applied on each empty chip in a range between 50 °C and 170 °C for all LSAPEs studied. The correction was performed only after the stage was stable at a temperature of 50 °C. Optimal sample placement was achieved with the assistance of a Leica M60 microscope and a CCD IC90 camera. Good sample-chip contact was achieved by cycling melting and cooling until reproducible data were obtained, and further confirmed by comparing the crystallization and melting temperatures obtained by DSC and by FSC at 60 °C min ^{1}. Data from DSC and from FSC agreed ±0.5 °C. The same thermal protocols implemented with DSC for isothermal crystallizations were used in FSC, except that the cooling and heating rates used were 2000 and 100 K/s, respectively. The overall crystallization rate was taken, as in DSC, as ($t_{0.5}^{1}$).

When the crystallization process becomes too slow there may be insufficient sensitivity in either FSC or DSC to capture the exothermic peak. In such cases, the isothermal crystallization at T_c was halted at different times and melting was recorded from T_c. The endotherms along the isothermal crystallization were used to determine crystallization rate values. This was done by taking the area of the melting peak as a function of crystallization time (t_c); a process which results in a sigmoidal curve from which we obtained the time to obtain half of the transformation, $t_{0.5}$.

2.3. Fourier-transform infrared spectroscopy (FTIR)

To collect kinetic data at the highest T_c for PE-18,18, the increase in area of the crystalline absorbance bands at 826, 921, and 1028 cm ^{1} was followed as a function of time [52]. The value of $t_{0.5}$ was extracted from the sigmoidal increase of the absorbance with crystallization time. Spectra were collected in real time during isothermal crystallization using a Thermo Scientific Nicolet iS50 spectrometer equipped with a DTGS KBr detector. OMNIC software was used for instrument control and peak analysis. The spectrometer was operated in absorption mode within wavenumbers of 4000 and 400 cm ^{1} with 2 cm ^{1} resolution. A thin film (~50 μm) of PE-18,18 was melted onto an ~0.2 mm thick KBr pellet, which was then placed inside a Linkam hot stage with ZnSe windows and connected to a TMS94 temperature programmer. The same thermal protocols as described above for DSC work were used to follow the isothermal crystallization at desired T_c.

2.4. Polarized optical microscopy (POM)

Polarized optical micrographs were collected using a BX51 Olympus microscope equipped with a DP72 Olympus digital CCD camera. CellSens software provided by Olympus was used to record and analyze isothermal spherulitic growth. The linear variation of the radius or diameter of at least three spherulites with increasing crystallization time at T_c was used to obtain growth rates, *G*. The same thermal protocols as for FTIR and DSC were followed; temperature was controlled using a Linkam hot stage.

2.5. X-ray analysis

Small-angle X-ray scattering (SAXS) and wide-angle X-ray diffraction (WAXD) patterns were simultaneously collected at room temperature using a Bruker Nanostar diffractometer with an Incoatec microfocus (IμS) X-ray source. The incident X-ray beam was a Cu K_α line with a wavelength $\lambda = 1.5418$ Å. To prepare isothermally crystallized samples for X-ray analysis, the above-mentioned thermal protocol was followed in the DSC, omitting melting after the isothermal crystallization step. Rather than melting, samples were instead quickly cooled from T_c to room temperature and brought to the X-rays. Baseline correction was applied to all SAXS patterns by subtracting the pattern of the empty sample holder. A Lorentz-correction was further applied to all SAXS patterns to determine the long period, *L*. The normalized one-dimensional correlation function (CF) was also applied to the first order SAXS peak and used to estimate *L* and the crystal thickness, l_c [53,54]. The method described by Goderis and discussed by us previously was used to extrapolate experimental SAXS data to 0 and infinite scattering vector, *q* [45,55]. The scattering vector is $q = 4\pi \sin\theta/\lambda$, with 2θ as the scattering angle.

2.6. Atomic force microscopy (AFM)

AFM height, amplitude, and phase images were collected using a Multimode 8 with a Nanoscope V controller operating in tapping mode in air under ambient conditions. Samples were scanned with silicon probes with a nominal resonant frequency of 77 kHz and spring constant 2.8 N m ^{1}. Lamellar thickness values were measured from flat-on lamellae in the height image mode. Samples were prepared for AFM analysis by placing a thin film on a single glass coverslip, melting, and crystallizing it isothermally at the desired T_c using a Linkam hot stage followed by quenching to room temperature.

3. Results and discussion

3.1. Overall crystallization rates

Crystallization exotherms for PE-48,48 (a), PE-32,32 (b), PE-18,18 (c), and PE-12,12 (d) as a function of increasing isothermal crystallization temperature, T_c, are shown in Fig. 1. The top panels (a) – (d), show data collected using DSC and the bottom panels, (e) – (h), show data collected at lower T_c using FSC. The very fast cooling rates possible with FSC enable expansion of the T_c range to lower values, which is useful for complete analysis of these LSAPEs. For all four LSAPEs in the low T_c range, the time for complete transformation increases with increasing T_c; the expected behavior following classical nucleation theory. This expected increase in crystallization time with increasing T_c is maintained over the entire range of T_c accessible via FSC and DSC in the shorter-spaced polyesters PE-12,12 and PE-18,18. In PE-48,48 and PE-32,32, however, an unusual behavior as a function of increasing T_c is observed, as demarcated by the red thermograms in Fig. 1(a), (b), and (f).

Looking first at PE-48,48 (in Fig. 1(a)), within a very small range of

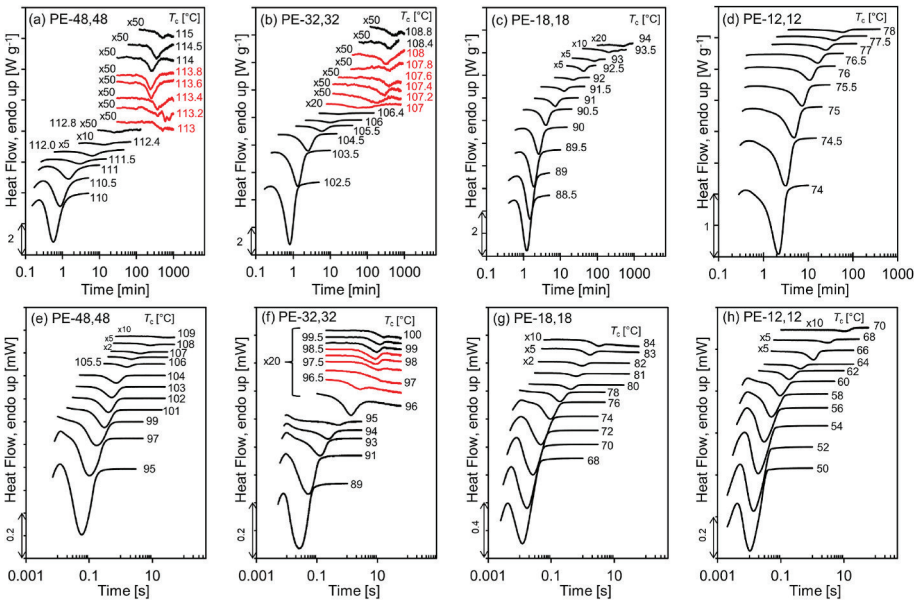

Fig. 1. Selected crystallization exotherms collected as function of time during isothermal crystallization at the indicated temperatures, T_c, for (a & e) PE-48,48, (b & f) PE-32,32, (c & g) PE-18,18, and (d & h) PE-12,12. Red thermograms highlight the reverse trend of the time to peak with increasing T_c for PE-48,48 and PE-32,32. (a–d) and (e–h) were collected using DSC and FSC, respectively. Data have been vertically shifted for clarity, and some exotherms are multiplied by a constant factor to show better the low heat flow transitions. (For interpretation of the references to colour in this figure legend, the reader is referred to the Web version of this article.)

T_c, from 112.8 to 113 °C (*i.e.*, only 0.2 °C), the crystallization time increases dramatically, from ~70 min to complete the full exotherm to > 800 min. Upon increasing T_c further from 113.2 until 113.8 °C, the crystallization time decreases to just 237 min, indicating a faster overall crystallization rate at higher T_c contrary to the predictions of nucleation theory. For T_c above 113.8 °C, crystallization time increases with T_c once again, thus returning to expected behavior. Interestingly, in PE-32,32, there are two inversions in the variation of peak time with increasing T_c, the first is observed in FSC, Fig. 1(f), over a T_c range of 96.5–98.5 °C, and the second is in the DSC data, Fig. 1(b), over a T_c range of 107–108 °C.

To illustrate the inversions in the temperature gradient of the crystallization time observed in Fig. 1 quantitatively, it is constructive to plot the overall crystallization rate, taken as $\ln(\frac{1}{t_{0.5}})$ where $t_{0.5}$ is the time to peak of the exothermic transformation (equivalent to half-time of crystallization), as a function of T_c. This is shown in Fig. 2 for all four

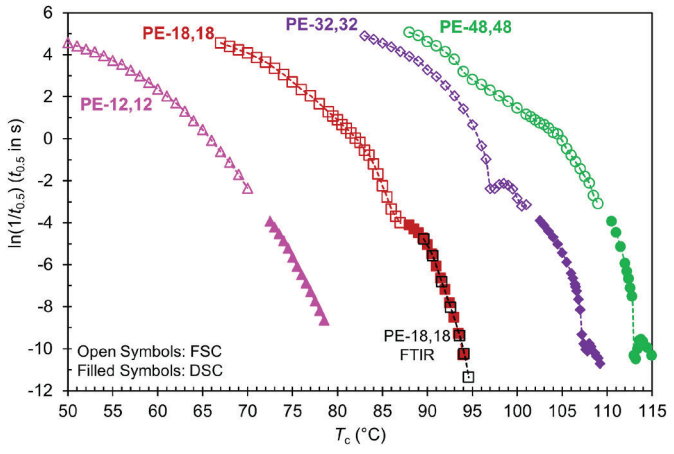

Fig. 2. Overall crystallization rate expressed as the natural logarithm of the inverse half-time of crystallization, $t_{0.5}$, as a function of T_c for PE-48,48 (green circles), PE-32,32 (purple diamonds), PE-18,18 (red squares) and PE-12,12 (pink triangles). Data collected using DSC are shown as filled symbols and those collected using FSC are shown as open symbols. Additional data for PE-18,18 were collected using FTIR and are shown as black, open squares. Dashed lines between data points are drawn to guide the eye to the observed trends. (For interpretation of the references to colour in this figure legend, the reader is referred to the Web version of this article.)

LSAPEs; data collected using FSC are shown as open symbols, while data collected using DSC are filled symbols. There is in general excellent agreement between the crystallization rate data collected using FSC and DSC. The latter demonstrates the advantage of using these techniques to extend the crystallization range to much lower temperatures while using fast cooling rates equivalent to those used in industrial processes. Minima in the overall crystallization rate are clearly observed for PE-32,32 at 97 and 107.8 °C, while a rate discontinuity and a deep minimum are observed for PE-48,48 at ~104 and 113.2 °C, consistent with the exotherms of Fig. 1.

In PE-18,18, there appears to be a discontinuity in the rate at T_c between 86 and 87 °C which could be associated with a shallow rate minimum. This behavior would not be visible in the exotherms of Fig. 1 (g) because by FSC the exothermic heat flow is small and spreads over a wide time range at these high temperatures, making it unviable to determine $t_{0.5}$. Instead, the FSC rate data shown in Fig. 2 for $T_c > 84.5$ °C in PE-18,18 were determined using the endotherm method described in the experimental part (see Fig. S2). Since this "break" in the variation of the crystallization rate with temperature occurs at the intersection of accessible T_c in FSC and DSC (corresponding to $t_{0.5}$ on the order of 1 min), it is not possible to rule out instrumental uncertainties in the determination of $t_{0.5}$ in this T_c range. However, support for the shallow crystallization rate minimum of PE-18,18 is that both FSC and DSC data shown in this region are repeatable, and that there is excellent agreement between the melting temperatures collected on heating at the same rate in both instruments. Conversely, in agreement with the crystallization rate data of PE-15 [37,38], the data for PE-12,12 show the typical monotonic decrease in overall crystallization rate with increasing T_c devoid of discontinuities or rate minima.

Similar minima to those seen in Fig. 2 for PE-48,48 and PE-32,32 in the overall crystallization and/or linear growth rates have been observed previously in various systems, including long-chain *n*-alkanes [41–43], methyl-terminated low molecular weight fractions of PEO [44], precision polyethylenes with bromine [47], long-spaced precision polyacetals [49,50], and short-spaced aliphatic polyesters [56–60]. Most recently, we observed crystallization rate minima in the short-long aliphatic polyester, PEB [40]. Although the precise interpretation of the minima or discontinuities in the crystallization rate vary among these systems, they have in common that the break in kinetics occurs concomitant with some polymorphic or crystalline structural transition.

Our previous studies have demonstrated that LSAPEs develop the same apparent orthorhombic unit cell in the whole range of T_c, above

and below the observed rate minimum in Fig. 2 [45,52]. Hence, the minima cannot be associated with a change in crystal packing. Furthermore, the same LSAPEs develop unlayered crystallites when rapidly cooled from the melt to room temperature. On heating, the unlayered crystals, with ester groups randomly arranged inside the crystals, transform to the ester-staggered layered type at temperatures between 45 and 60 °C [52]. Since in this range the temperatures are much lower than where the rate minima are observed in Fig. 2, the rate minima cannot be related to the unlayered-layered transition either. Moreover, the two rate minima shown in Fig. 2 for PE-32,32 are analogous to the two minima observed in PEB which we associated with a change between quantized crystal thicknesses with increasing T_c, [40]. Hence, the PE-32,32 minima are likely associated with a similar transition to thicker crystals with an integer number of ester layers.

Interestingly, the data of Fig. 2 also indicate that not only is the rate of crystallization displaced to lower T_c with decreasing methylene spacer, but the crystallization rate minima of symmetric LSAPEs become more difficult to observe with decreasing methylene sequence length. Namely, while two rate minima are observed for PE-48,48 and PE-32,32, only one is observed for PE-18,18 and none for PE-12,12. Some rationale for such a trend is found from estimates by linear extrapolation of the observed temperatures at the rate minima versus number of carbons between consecutive esters (Fig. S3). The estimated values for the high T_c rate minima are ~103 and ~101 °C for PE-18,18 and PE-12,12 respectively, which from Fig. 2 would be too high temperatures for the minima to be experimentally observed. Nonetheless, we tried to acquire rate data for PE-18,18 at higher T_c using FTIR with the method described in the experimental section (Fig. S4). The results are added as open squares in Fig. 2 and match the rate data obtained by DSC. Clearly, the rates for $T_c > 95$ °C become unduly long as those T_c are only ~2 °C below the observed melting peak. A similar linear extrapolation yields an estimate of 85 °C for the low T_c rate minimum of PE-12,12 which from Fig. 2 is also a too high T_c. Hence, we conclude that with decreasing CH_2 spacer there is a trend toward shallower and eventually disappearing crystallization rate minima in symmetric LSAPEs.

Schick and coworkers used FSC to study the overall crystallization rate of iPP and different polyamides at high undercooling and detected a minimum in the rate at temperatures (T_c) approaching the glass transition temperature (T_g) [61,62]. The systems studied develop a mesomorphic structure when solidified from the melt at large undercooling and a more ordered crystal form at lower undercooling. The observed rate minimum occurs at the transition temperature between the crystal and the mesophase and was interpreted as a change from heterogeneous to homogeneous nucleation. Support for this argument were Avrami exponents (n) for T_c above and below the rate minimum changing from 3 to 4 respectively and a morphological change from spherulitic to a nodular structure. It was perceived that at high T_c heterogeneities commonly present in polymer melts act as athermal nuclei and polymer crystals grow from these sites as spherulites ($n = 3$), while at T_c approaching T_g the energy barrier for developing polymer self-nuclei may be sufficiently low to generate profuse nuclei at a constant rate ($n = 4$). The experimental rate data were fitted with two bell curves, each corresponding to the range of temperatures where the development of crystallinity was governed by polymer nucleation (T_c close to T_g) or growth from the heterogeneous nuclei (high T_c) [62,63].

Based on T_g values of poly ε-caprolactone (60 °C) and linear polyethylene (120 °C), the T_g of the four LSAPEs studied here is estimated at ~ 80 °C, therefore, all crystallization rate data of Fig. 2 are obtained at T_c well above the polyesters' T_g; hence, a change from the usual heterogeneous nucleation ($n = 3$) to homogeneous nucleation ($n = 4$) is not expected. Furthermore, the presence of multiple minima cannot be explained by the above single change in type of nucleation. Nonetheless, we carried out Avrami analysis of exotherms collected at T_c below and above the rate minima. The procedure, plots and tabulated Avrami exponents can be found in the supplementary documentation (Fig. S5 and Table S1). As expected, for all LSAPEs the Avrami exponents at the highest T_c are ~3, or the expected value for heterogeneous nucleation and three-dimensional growth. There is also a tendency to fractional exponents ($2.2 < n < 2.7$) at the lowest T_c recorded by FSC denoting that at such high undercooling growth may be affected by diffusion in the highly viscous melt [64,65]. Regardless, the n exponent remains unchanged at T_c above and below the LSAPEs rate minima. Hence, we conclude that the observed crystallization rate minima in LSAPEs must be due to factors other than a change in nucleation type. As mentioned earlier, the minima are most probably related with a change in crystal thickness to a quantized number of ester-ester repeats, as found for PEB [40].

3.2. *Melting of crystals formed below and above the crystallization rate minima*

Fig. 3 presents melting endotherms collected on heating after isothermal crystallization at the indicated T_c. The crystallization time at each T_c was limited to that required for the exotherm to complete. In other words, samples were not annealed beyond their primary crystallization. In doing so, step thickening known from our previous work to occur in PE-48,48 on isothermal annealing [45], is minimized, and we may investigate the melting behavior as a function of T_c independently from the thickening mechanism. The red thermograms in Fig. 3(a), (b), and (f) correspond to the region where the minima in crystallization rates were observed in Fig. 1.

While single endotherms are observed after low T_c crystallizations in FSC, for PE-48,48 (Fig. 3(a)), there is a clear transition from T_c of 112.8–113 °C, from a single melting endotherm at ~114 °C to double melting peaks at ~114 and ~118 °C. We know from our prior work that the lower and higher melting temperatures correspond to layered crystallites with non-integer (<3 monomer repeats) and integer (3 repeats) thicknesses, respectively [45]. Increasing T_c further by only 0.2 °C, to 113.2 °C, integer layered crystals are the dominant type, and at 113.4 °C, only integer layered crystals remain. Qualitatively, we observe in Fig. 3(a) a decrease in heat of melting at T_c approaching 113 °C from below, and a significant subsequent increase at $T_c \geq 113.2$ °C; this enthalpic change is consistent with the change in the area of the exothermic peak at the same T_c (see Fig. 1(a)). The narrow T_c range where metastable non-integer transition to stable integer layered crystals corresponds directly to the crystallization rate minimum as seen in Figs. 1 and 2, thus providing clear evidence that the minimum in kinetics is related to this transition. Furthermore, the sharp decrease in heat of melting and heat of crystallization at the transition points to the same mechanism postulated to explain the rate minima found in PEB [40]. Namely, that the nucleation and growth of the integer layered crystals are frustrated by the kinetically favored non-integer layered form at T_c transitioning between the two structures.

In Fig. 3(a), the high temperature melting peaks (at ~117 °C) seen at the lowest T_c recorded by DSC in PE-48,48 are due to recrystallization during heating. On heating, the initial non-integer crystals melt at ~113 °C and recrystallize into the integer form that further melts at ~117 °C. Recrystallization becomes less prominent as the non-integer layered crystals gain stability at higher T_c as illustrated by the progressive disappearance of the melting at ~117 °C in the T_c range from 110 to 112 °C in Fig. 3(a). Double melting is not apparent in the lower T_c FSC data since the heating rate (100 K/s) is fast enough to suppress recrystallization.

Due to the formation of a mixture of integer and non-integer crystallites in the low T_c region and fast recrystallization of non-integer to integer crystals on heating [45,52], the endotherms of PE-32,32 show less dramatic double melting features than those of PE-48,48 (Fig. 3 b and f). The shoulder at 98 °C and melting peak at 107 °C in the low T_c range of both panels, correspond to melting of non-integer crystals that on heating melt and recrystallize into integer crystals that further melt at 105 °C and 112 °C respectively. The two low temperature melting peaks disappear at T_c approaching the rate minima, thus confirming that the

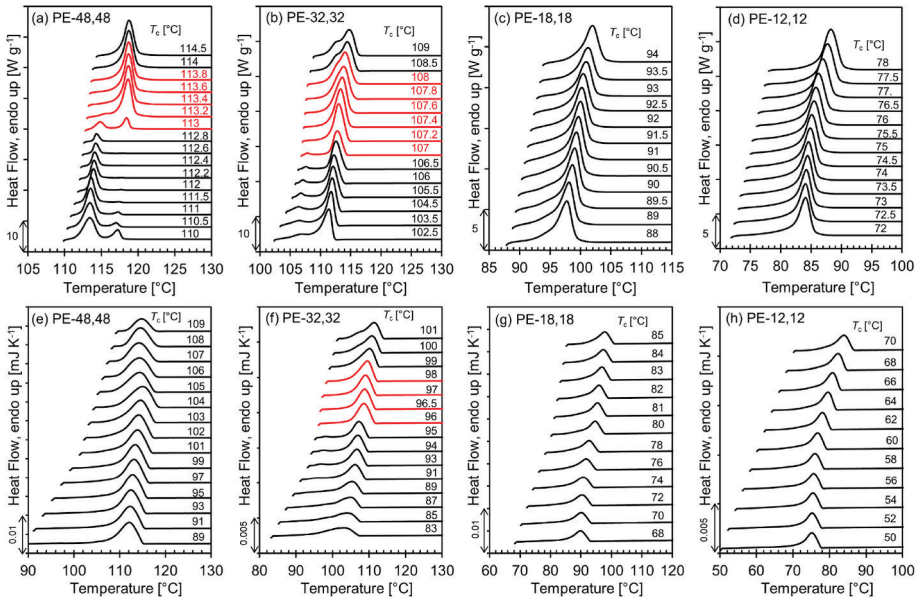

Fig. 3. Selected melting endotherms after isothermal crystallization at the indicated T_c for PE-48,48 (a, e), PE-32,32 (b, f), PE-18,18 (c, g), and PE-12,12 (d, h). Top thermograms are collected in DSC on heating at 10 °C min^{-1}, bottom thermograms are collected in FSC at 100 K/s. Red thermograms in (a), (b) and (f) indicate the transition from non-integer to integer layered crystals. (For interpretation of the references to colour in this figure legend, the reader is referred to the Web version of this article.)

rate minima are associated with the transition from non-integer to integer crystallites.

In contrast, for PE-18,18 and PE-12,12, Fig. 3(c) – (d) and (g) – (h), a single melting peak is apparent at all T_c, with the expected gradual increase in melting point with decreasing undercooling. Only for the data of PE-18,18 at T_c transitioning from FSC to DSC data, or for T_c from 85 to 88 °C where we observe the discontinuity in the rate, is the melting point increasing from 94 to 97 °C, thus pointing to an analogous transition to a thicker quantized crystal structure.

The metastability of non-integer crystals is further documented by analyzing the melting behavior of isothermally formed crystals as a function of crystallization time. An isothermal transformation from non-integer to integer layered crystals was observed previously for PE-48,48 with increasing crystallization time [45]. A similar feature is present in PE-32,32, as can be seen in Fig. S6. Interestingly, step thickening appears to be complete in PE-32,32; the non-integer peak disappears

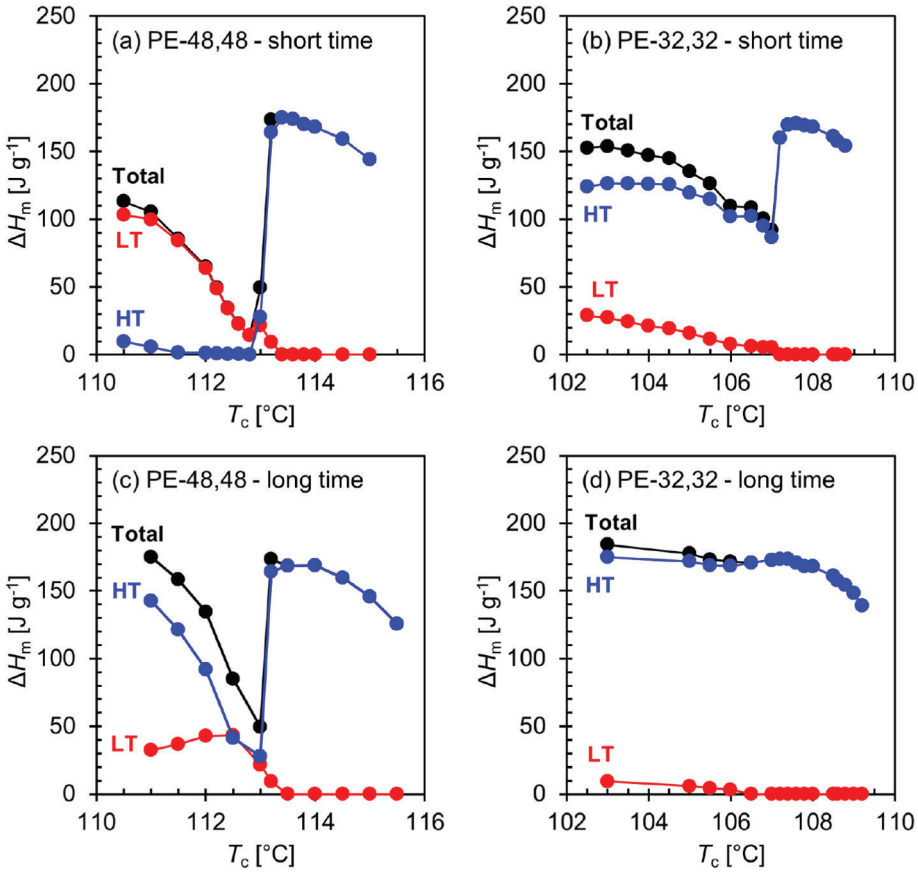

Fig. 4. Heats of melting (ΔH_m) for PE-48,48 (a, c) and PE-32,32 (b, d) after crystallizing at T_c for "short" crystallization times ((a), (b) – only long enough to complete full exotherm) and "long" crystallization times ((c), (d) – on annealing at T_c beyond the complete exotherm for (c) all at 1000 min, and (d) 800 min for T_c (103–107.5 °C) and 1000 min for T_c (108–109 °C)). The total, lower temperature (LT), and higher temperature (HT) heats of melting are shown as black, blue, and red data points, respectively. For PE-48,48, the minimum in ΔH_m is preserved even after long annealing times (~1000 min), while for PE-32,32 the total ΔH_m is mostly flat upon annealing up to very high values of T_c. The lines between data points are drawn to guide the eye to the observed trends. (For interpretation of the references to colour in this figure legend, the reader is referred to the Web version of this article.)

entirely upon annealing for relatively short times (~10 h). Complete transformation is unreasonable to achieve in PE-48,48, due to the extraordinarily long time that doing so would require (e.g., >70 h, at T_c = 111 °C) [45]. That PE-32,32 seems to isothermally transform more easily from the non-integer to the integer layered form explains why the decrease in heat of melting near the transition (seen qualitatively in Fig. 3(b) and in the exotherms of Fig. 1(b)) is not as pronounced in PE-32,32 as it is in PE-48,48. Thus, these data demonstrate further the impact of the length of the methylene spacer between esters on the crystalline structure. In symmetric LSAPEs, a shorter spacer facilitates either the initial formation of stable integer crystallites or a faster thickening of non-integer crystals toward the more stable integer form.

An easier transformation from non-integer to integer layered crystals is expected to reduce the impact of the frustration on the heat of melting and the overall crystallization rate at T_c transitioning between both structures. This is corroborated by examining the heat of melting upon increased isothermal annealing time. Shown in Fig. 4(a) and (b) are the heats of melting for PE-48,48 and PE-32,32 corresponding to the endotherms of Fig. 3(a) and (b), which were not subject to isothermal annealing. Clearly, there is a minimum in the total heat of melting at the same T_c of the minimum in crystallization rate for both PE-48,48 and PE-32,32 as observed qualitatively in Fig. 3. This feature is reminiscent to the extinguished crystallization observed in long-spaced aliphatic polyacetals at the transition between high temperature polymorphs [49]. In that case, nucleation and growth of Form II is frustrated by the kinetically favored Form I that develops only up to small content due to the extremely low undercooling for this form. The result is a total heat of fusion that is only ~ one-fifth the value obtained at lower T_c. The heat of fusion recovers upon increasing T_c beyond the transition in the range where pure Form II develops.

Due to large difference in nucleation energy barriers between Form I and Form II in the case of the polyacetals, crystallizing at T_c of the rate minimum for longer times beyond the exothermic peak does almost nothing to increase the heat of melting, which is the reason for the use of the "extinguished crystallization" terminology [49]. The difference in nucleation barriers between quantized crystal thicknesses is not expected to be as high for LSAPEs. Metastable polyester crystals with thicknesses between two quantized forms would thin or thicken to a lower free energy state to acquire higher stability. As seen in Fig. 4, the dynamics of the latter are faster as the methylene spacer decreases in symmetric LSAPEs. Although the minimum in the heat of melting is clearly maintained on annealing for about 1000 min in PE-48,48, the transformation from non-integer (LT) to integer (HT) layered crystals is evident in Fig. 4(c). Furthermore, in PE-32,32, the heat of melting recovers to be nearly constant with T_c after longer isothermal crystallization times, consistent with the observation that the isothermal step thickening is completed within relatively short annealing times in this LSAPE (Fig. S6).

3.3. Overall morphology and isothermal linear growth rates

Overall crystallization rates followed by DSC, FSC, or FTIR encompass both nucleation and growth kinetics. Thus, to ascertain whether the minima in the overall crystallization rate occur in the nucleation or growth (or both), we investigate growth rates separately using polarized optical microscopy. A representative set of optical micrographs for PE-48,48 collected at temperatures below and above the observed rate minimum at T_c of 113 °C ($T_{c,min}$) for the indicated elapsed time is given in Fig. 5. The overall morphology is spherulitic with positive birefringence. A well-defined Maltese cross is apparent at T_c above $T_{c,min}$, while below $T_{c,min}$ it is somewhat less clear due to higher nucleation density. Interestingly, at the $T_{c,min}$ of 113.0 °C, the nucleation density decreases quite significantly, only to increase again at $T_c \geq 113.4$ °C, thus denoting an inversion in the temperature gradient of the nucleation rate. Furthermore, at the $T_{c,min}$, open and irregularly shaped spherulites indicate extremely slow growth at this temperature. Remarkably, increasing T_c from $T_{c,min}$ by only ~0.4 °C returns the viewing area to a faster development of a distinct spherulitic morphology. Hence, these morphological details point toward inversion in the temperature coefficient of both the nucleation and growth rates of PE-48,48 and explain the observed pronounced rate minimum in the overall crystallization rate of Fig. 2.

An interesting observation is that it is only at the transition between the non-integer and integer layered structures (at $T_{c,min}$ of 113 °C ± 0.2 °C) when the nucleation density shows a strong decrease and the spherulitic morphology becomes irregularly shaped, while the spherulitic morphology below and above the transition remains unchanged. These morphological features are equivalent to those recently observed in PE-2,13 [40], and support nucleation barriers between structures at T_c above and below the rate minimum that, albeit different, may not differ as much as, for instance, Forms I and II of polyacetals [49,50]. In the latter, besides a morphological change, there is a dramatic decrease in nucleation density at T_c above the transition between forms. With expected relatively small difference in nucleation barriers between the non-integer and integer layered crystalline structures of LSAPEs, the inversions in the temperature coefficient of the crystallization and nucleation rates can be explained primarily by the self-poisoning feature [41–43].

The morphology of PE-32,32, PE-18,18, and PE-12,12 is also spherulitic. In these shorter spaced LSAPEs, the nucleation density is

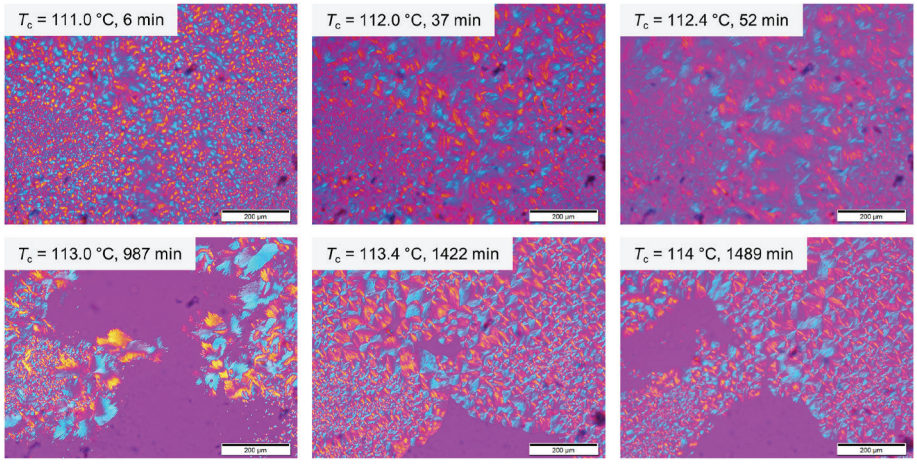

Fig. 5. Polarized optical micrographs obtained during isothermal crystallization of PE-48,48 at the indicated T_c after the indicated elapsed time. Scale bars represent 200 μm.

quite high, and no changes in morphology or nucleation are evident with T_c, even near the $T_{c,min}$ of 107.8 °C in PE-32,32. The relatively smaller content of non-integer layered crystals that develops isothermally in PE-32,32 (see melting endotherms of Fig. 3(b) in the low T_c DSC range) likely explains the lack of morphological change near the transition from non-integer to integer layered crystals in this polymer. Neither the lower $T_{c,min}$ of PE-32,32 at 97 °C nor the apparent discontinuity feature at ~86 – 87 °C in PE-18,18 observed in FSC are accessible for polarized microscopy imaging. The fastest cooling rate of the Linkam hot stage used for temperature control is well below the cooling rate needed to avoid crystallization prior to reaching such low T_c range.

As mentioned in the introduction, the premise of the self-poisoning framework is a temporary blockage at the crystal growth surface by deposition of a kinetically favored but metastable structure. Therefore, additional evidence to support self-poisoning at the rate minima should be a retardation in the growth rate of the more stable crystalline form at temperatures approaching the rate minima from above [43,47]. Hence, if in addition to some difference in nucleation barriers, self-poisoning is at play in the LSAPEs, we expect to observe an analogous minimum in the isothermal linear growth rates (G). Fig. 6 displays ln(G) as a function of T_c for each of the LSAPEs. As shown, there are minima in the G of PE-48,48 and of PE-32,32 at T_c of 113.0 °C and 107.6 °C respectively, the same temperatures where the minima were found in the overall crystallization rates measured by DSC and where the spherulitic growth and overall morphology appeared rougher and more disorganized respectively. Analogous to the DSC results, no minimum in G is evident over the accessible T_c range for PE-18,18 or PE-12,12. Hence, the diminishing ability to observe a rate minimum with decreasing CH_2 spacer length in LSAPEs found in the overall crystallization rates, is also present in the growth rates of these polyesters.

The rate minima found in Figs. 2 and 6 fall closely in line with that found for *n*-alkanes, PEO fractions, and PE-2,13 where the crystal phase is maintained with increasing T_c and the structural change above and below the rate minimum is a step difference in crystal thickness. Adopting the same framework to explain the crystallization kinetics of these LSAPEs, we expect a step increase in crystal thickness at T_c across the rate minima. Hence, crystal thicknesses for T_c below and above the minimum are analyzed next by SAXS.

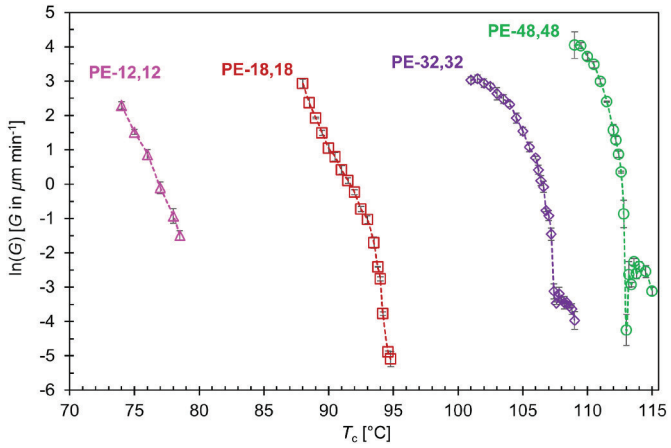

Fig. 6. Natural logarithm of the isothermal linear growth rates, G, as a function of T_c for PE-48,48 (green), PE-32,32 (purple), PE-18,18 (red) and PE-12,12 (pink). Error bars indicate ± one standard deviation from the average of measurements obtained independently from at least three spherulites. Dashed lines between data points are drawn to guide the eye to the observed trends. (For interpretation of the references to colour in this figure legend, the reader is referred to the Web version of this article.)

3.4. Discontinuous changes in long spacing and lamellar thickness

Fig. 7 displays Lorentz-corrected SAXS patterns for PE-48,48 (a) and PE-32,32 (b) collected after isothermal crystallization at T_c below (black patterns) and above (red patterns) the rate minima ($T_{c,min}$). The corresponding WAXD patterns are unchanged (Fig. S7). Note that $T_{c,min}$ refers to the high T_c minimum observed via DSC. As done for the melting endotherms of Fig. 3, samples were crystallized only long enough for the complete exotherm to develop, thus minimizing step thickening which occurs for longer annealing times at $T_c < T_{c,min}$. There is a clear shift of the scattering vector toward lower values (longer spacing) with only a 1 °C increase in T_c for both PE-48,48 and PE-32,32. The T_c at which the shift occurs coincides directly with $T_{c,min}$ in both polyesters, indicating that the change in long period ($L = 2\pi/q_{peak}$) is related to the minimum in the crystallization rate. The shift in q_{peak} of PE-48,48 is about twice that for PE-32,32; in the former, q_{peak} changes from ~0.035 to 0.027 Å $^{-1}$, while in the latter the shift is only from ~0.030 to 0.026 Å $^{-1}$. This corresponds to an increase in long period of ~60 Å for PE-48,48 and ~30 Å for PE-32,32 (see Fig. S8 for quantitative long period data as a function of T_c). Also consistent with our earlier results, patterns for PE-18,18 and PE-12,12 (shown in Fig. 7(c) and (d) respectively) show a small gradual increase in long periodicity over the entire range of accessible T_c via DSC.

The normalized one-dimensional correlation function (CF) was applied to the data of Fig. 7 to extract the core lamellar thickness (l_c). Examples of CF are given in Fig. S9. The results are shown in Fig. 8(a) for PE-48,48 (green), PE-32,32 (purple), PE-18,18 (red) and PE-12,12 (pink). In PE-48,48 and PE-32,32, $T_{c,min}$ is demarcated with a dashed vertical line, and the values for l_c below and above $T_{c,min}$ are closed and open circles, respectively. The l_c of PE-12,12 increases continuously with T_c as expected with decreasing undercooling, and the same trend is found for PE-18,18 for $T_c > 90$ °C. For both PE-48,48 and PE-32,32, there is a discontinuous step increase in l_c from below to above the $T_{c,min}$. The increase is ~30 Å for PE-48,48 (from ~120 to 150 Å) and about 20 Å for PE-32,32 (from ~130 to 150 Å). Thus, it is clear that indeed the crystals undergo a discrete increase in thickness from below to above $T_{c,min}$ in both PE-48,48 and PE-32,32.

With the reflection identified as the ester-ester layer distance in the middle-angle X-ray patterns, d, we calculated the number of ester-ester layers (l_c/d) that correspond to the crystal thicknesses shown in Fig. 8 (a). Values of d are ~16, 20.8, 35.3, and 48.0 Å for PE-12,12, PE-18,18, PE-32,32, and PE-48,48, respectively, see Fig. S10 [52]. The number of ester-ester layers is shown in Fig. 8(b) for each LSAPE. With increasing T_c, PE-48,48 crystals thicken from ~2.5 to 3 ester-ester layers at $T_{c,min}$. Similarly, crystals of PE-32,32 thicken from ~3.5 to 4 ester-ester layers. PE-18,18 and PE-12,12 crystals contain ~6 and 8 – 10 ester-ester layers respectively, implying that placing the ester groups at the basal surfaces of the crystals must be easier in shorter-spaced LSAPEs. That the step change in crystal thickness from a non-integer to an integer number of ester-ester repeats occurs in both PE-48,48 and PE-32,32 at the corresponding $T_{c,min}$ strengthen conclusions reached in our earlier work for PEB [40]. Namely, that the crystallization rate minima in LSAPEs occurs as a result of reaching a quantized number of monomer units in the crystal thickness.

In addition to the step change in long period and crystal thickness, another change evident in the SAXS patterns of PE-48,48 (Fig. 7(a)) is the appearance of the second order long period reflection at $T_c > T_{c,min}$. This feature indicates an improvement in symmetry for the high temperature, integer layered crystals with respect to the lower temperature, kinetically favored, non-integer layered type. PE-32,32 develops a mixture of non-integer and integer layered crystals at $T_c < T_{c,min}$, as inferred by the presence of the second order long period reflection even for low T_c. Such a mixture of non-integer and integer layered structures in PE-32,32 at all T_c is consistent with the melting endotherms of Fig. 3 (b). Moreover, a mixture of structures at $T_c < T_{c,min}$ explains the smaller shift in q_{peak} for PE-32,32 than PE-48,48 at the transition.

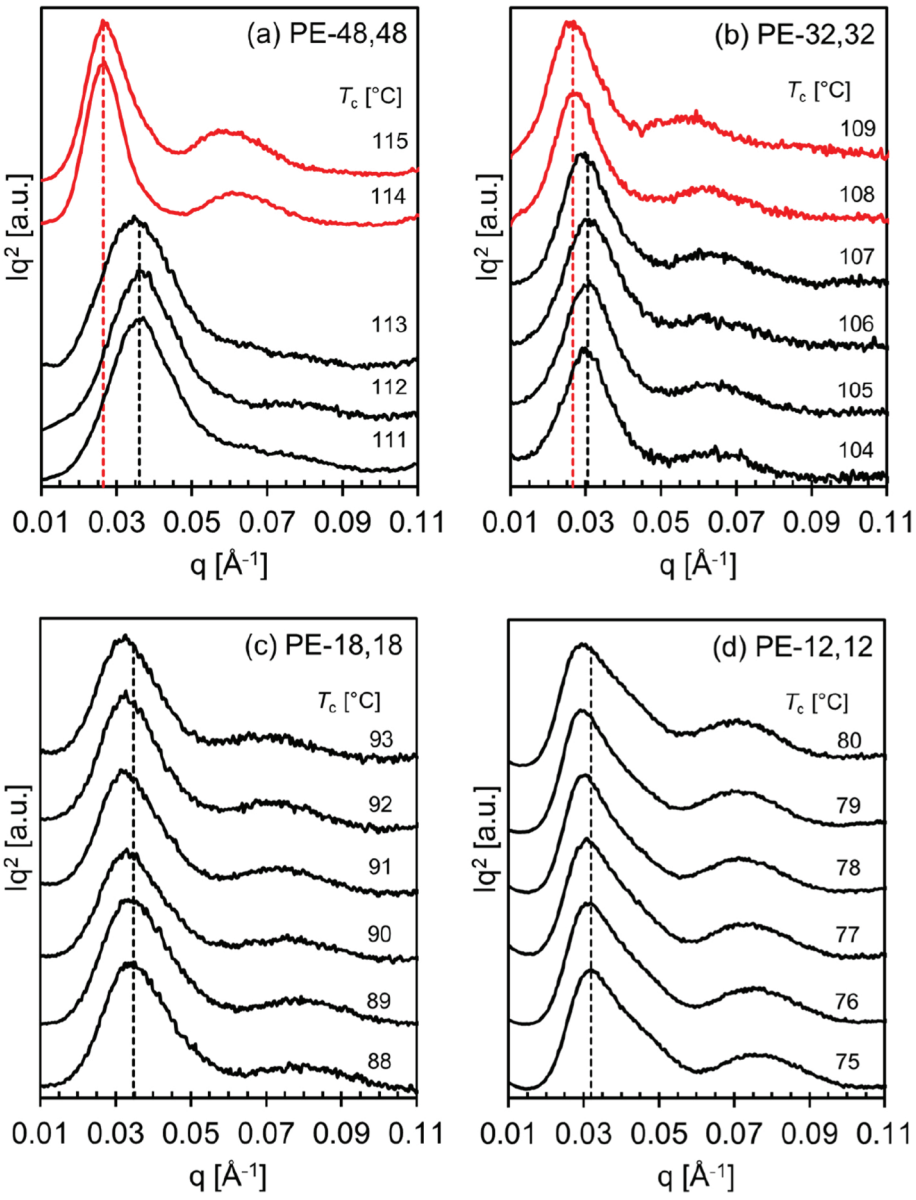

Fig. 7. Lorentz-corrected small-angle X-ray scattering (SAXS) patterns for PE-48,48 (a), PE-32,32 (b), PE-18,18 (c), and PE-12,12 (d) collected at room temperature after isothermal crystallization at the indicated T_c. Red patterns in (a) and (b) highlight the shift in the long period reflection above the transition from non-integer to integer layered crystals. Vertical dashed lines are drawn also to highlight this shift. Patterns have been vertically shifted for clarity. (For interpretation of the references to colour in this figure legend, the reader is referred to the Web version of this article.)

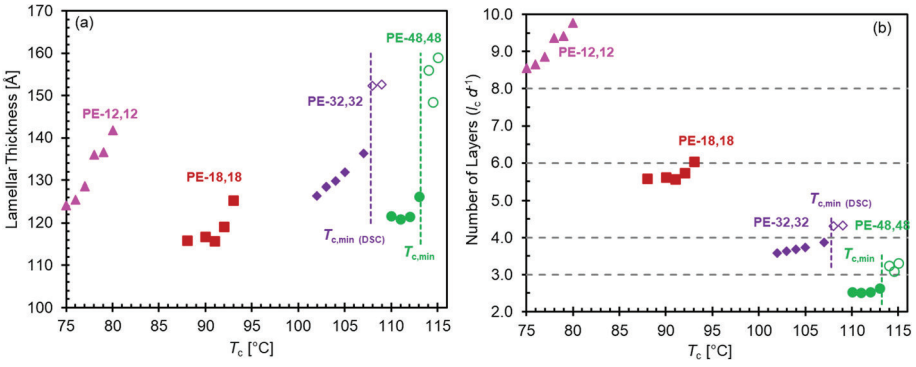

Fig. 8. (a) Core lamellar thickness (l_c) calculated using the normalized one-dimensional correlation function and (b) estimated number of ester-ester layers as l_c divided by the observed layer distance, d, as a function of T_c for PE-48,48 (green circles), PE-32,32 (purple diamonds), PE-18,18 (red squares), and PE-12,12 (pink triangles). Below $T_{c,min}$, (dotted, vertical lines) data are expressed as filled circles while above $T_{c,min}$ data are shown as open circles. Dashed horizontal lines in (b) represent integer numbers of ester-ester layers and are drawn to guide the eye. (For interpretation of the references to colour in this figure legend, the reader is referred to the Web version of this article.)

AFM was also used as a direct technique to corroborate the increase of lamellae thickness at $T_{c,min}$. Height and amplitude AFM images are shown in Fig. 9 for PE-48,48 (left) and PE-32,32 (right) for T_c below and above $T_{c,min}$ (top and bottom images, respectively). The morphology is clearly lamellar, as expected, and many of the lamellae are flat-on, as can be seen clearly in the amplitude images. The thickness of flat-on lamellae can be directly measured using the AFM height images. Values of l_c averaged over several images are listed in the captions of Fig. 9. As shown, the l_c increases from ~134 to 163 Å in PE-48,48, while in PE-32,32 the increase is from ~113 to 177 Å, giving further evidence

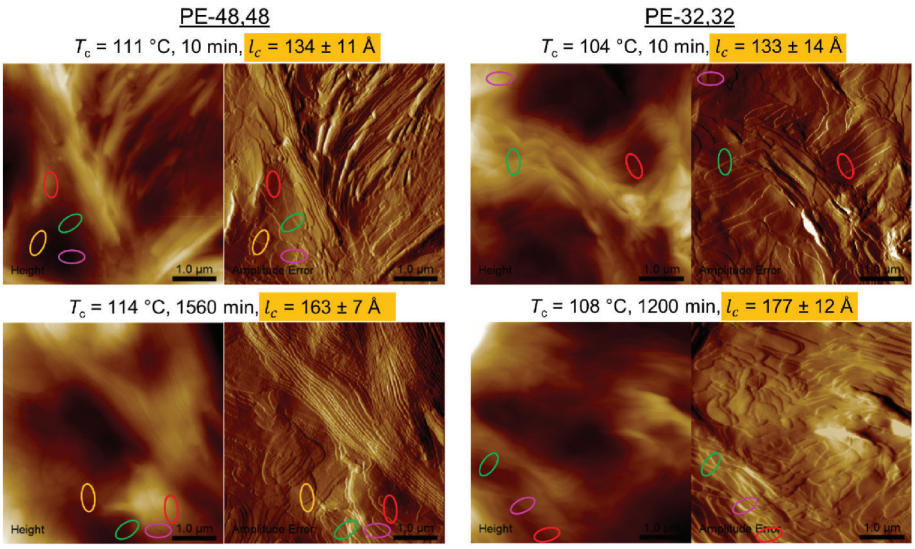

Fig. 9. AFM height and amplitude images for PE-48,48 (left) and PE-32,32 (right) after isothermal crystallization at the indicated T_c below (top) and above (bottom) $T_{c,min}$. Lamellar thicknesses, l_c, and values of one standard deviation from the average over several images are highlighted in yellow. Scale bars correspond to 1 µm. Colored ovals throughout the images indicate examples of areas in which the lamellar thickness was measured. (For interpretation of the references to colour in this figure legend, the reader is referred to the Web version of this article.)

to support the discontinuous thickening from below to above $T_{c,min}$. Note as well that there are no evident changes in the lamellar morphology accompanying the change in l_c. PE-18,18 has a similar lamellar morphology as that of PE-48,48 and PE-32,32, with a lamellar thickness that does not change appreciably with T_c, as expected (see Fig. S11).

3.5. *Metastable non-integer segments attaching at the growth front of integer layered crystals*

Based on the kinetic, morphological, and structural behavior as a function of T_c for LSAPEs detailed in the previous sections, we have demonstrated in high molecular weight polymers that a discrete step change in lamellar thickness causes a rate minimum in both the overall crystallization and crystal growth rates. In LSAPEs, the step change in crystal thickness is driven by the need to place the ester groups at the basal surfaces to reach more stable crystallites and is intrinsic to the regularity of the ester placement in a polyethylene-like chain. The latter is analogous to the behavior of long-chain *n*-alkanes, where the drive to place end groups at the crystal surfaces leads to discrete, quantized changes in crystal thickness with decreasing undercooling; for instance, from once-folded to extended *n*-alkane chain crystals. That we observe the minimum in the growth rate of the LSAPEs points toward a blocking effect at the crystal growth front of the more stable form by stems of the kinetically favored thinner form. In this section, we explain this blocking effect on the basis of self-poisoning, as has been described in detail for the *n*-alkanes [43], precision bromine containing polyethylenes [47], and polyester PEB [40].

Fig. 10 shows a schematic representation of the frustration at the growth front of an integer layered crystal by the deposition of metastable non-integer stems in LSAPEs at $T_{c,min}$. Illustrations are overlapped with the crystal growth rate data corresponding to PE-48,48 of Fig. 6 as an example to help demonstrate the proposed mechanism. For temperatures above the melting point of the non-integer layered crystals (T_m = 113 °C), only integer layered crystals can achieve productive growth. As the non-integer layered crystals are kinetically favored, when approaching their melting temperature from above, for 113 °C < T_c < 114 °C, the probability of deposition of those thinner, non-integer segments onto the growth surface of the thicker crystals increases. However, there are two factors that retard growth in such event. On one hand, the non-integer attached structure is metastable, it would quickly begin to thicken to complete the ester layer and gain stability by placing the ester groups at the surface of the crystal [45]. On the other hand, given that continuous growth of the non-integer crystals will not be

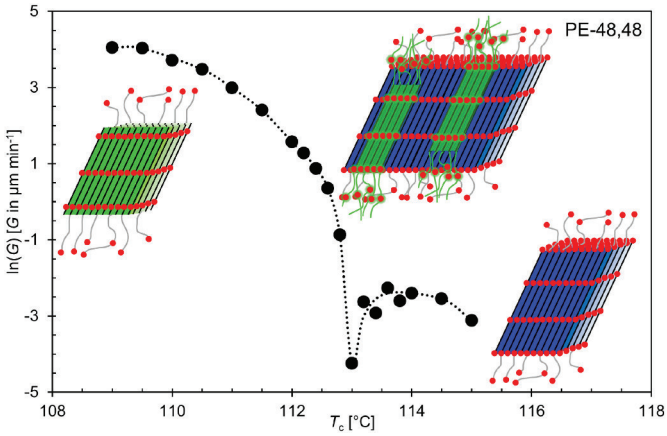

Fig. 10. Schematic representation of self-poisoning in LSAPEs overlapped with crystal growth rate for illustrative purposes. For low and high T_c, crystals form in the non-integer and integer layered type, respectively. Near the rate minimum, $T_{c,min}$, at the transition between non-integer and integer layered structures, non-integer layered stems block the growth front of the growing integer structure. Stems must thicken to the full length of the integer layered structure before growth can proceed uninhibited, thus causing a retardation in the growth rate.

productive above their melting point, growth of the integer layered crystal will temporarily stop until the thinner segments thicken by extension in the chain axis to complete the crystalline layer. The dynamics of the thickening event in the whole growth front will take some time causing a retardation in the linear growth rate, as shown. A similar mechanism may reduce the number of the initial nuclei.

Below their melting point, not only do the metastable but kinetically favorable non-integer layered crystals develop at a much faster rate (left side of rate minimum in Fig. 10) but the dynamics for isothermal thickening slow down with decreasing T_c [45]. The latter explains the non-integer crystal thicknesses observed in Fig. 8 at T_c < $T_{c,min}$. Although the schematics in Fig. 10 are shown for PE-48,48 crystals transitioning from ~2.5 to 3 layers, the same rationale applies to explain the rate minima in the low T_c region and for the rest of the LSAPEs. The observed LSAPE rate minima are associated with a transition toward a quantized number of monomer units in the chain axis of the crystallites.

As shown in Figs. 2 and 6 respectively, the inversion in the temperature coefficient of both the overall crystallization rate and the linear

growth rate is extraordinarily deep in PE-48,48; in PE-32,32 the high T_c minimum is not nearly so dramatic, it becomes just a discontinuity in PE-18,18, and is entirely absent for PE-12,12. It seems then, that the rate minimum becomes more difficult to see with decreasing methylene spacer length. This finding is consistent with arguments made by Ungar et al. regarding the behavior of $C_{390}H_{782}$, which shows three minima in its growth rate corresponding to the transitions between extended and once-folded (E-F_2), once-folded and twice-folded (F_2-F_3), and twice-folded and thrice-folded (F_3-F_4) crystals [43]. They found that while the growth rate minima at the E - F_2 and F_2 - F_3 transitions were deep in this *n*-alkane, the minimum at the F_3 - F_4 transition was comparatively shallow. Ungar *et al.* explained this behavior by considering the decrease in the difference between stem lengths at each of the three transitions. The E - F_2 stem length difference is 20.8 nm, F_2 - F_3 is 7.0 nm, but the difference between stem lengths at the F_3 - F_4 transition is just 3.5 nm. Since the result of self-poisoning is the lack of productive growth associated with the attachment of longer stems onto the incorrectly attached shorter ones, the authors argued that there must be some stem length difference for which this rule is not rigorously followed, making self-poisoning inoperable at those conditions [43]. Ungar *et al.* also found that the rate minimum becomes shallower with decreasing *n*-alkane length, in agreement with findings in the series of precision bromine polyethylenes [47]. As the methylene sequence becomes shorter, from 20 to 8 methylenes between consecutive bromine substitutions, the minimum in growth rate becomes shallower. In fact, for the precision bromine polyethylene spaced by 8 methylenes, only a discontinuity, and no minimum, was observed [47].

Applying the above rationale to the LSAPEs studied here, the difference in lamellar thickness between non-integer and integer layered crystals is (as demonstrated in Fig. 9(a)) ~30 Å in PE-48,48, and only ~20 Å in PE-32,32 (for the high $T_{c,min}$ from ~3.5 to 4 ester-ester layers). It is conceivable then, that the rate retardation effect of a 20 Å stem length difference would be considerably less than a difference of 30 Å. Additionally, since the most likely mechanism for alleviating the poisoning effect in the LSAPEs is thickening toward the integer layered structure, it is logical that thickening by 20 Å can be accomplished in a smaller time frame than a thickening of 30 Å (as corroborated by the melting endotherms as a function of time for PE-32,32 in Fig. S6 and in our prior work for PE-48,48 [45]), thus limiting the impact of the attachment of the wrong structure on the rate. The above rationale is consistent with a weaker crystallization rate minimum in PE-18,18 and the lack of any clearly apparent minimum in PE-12,12. Since the distance between consecutive ester groups in PE-18,18 is only ~23 Å (~16 Å in PE-12,12), the difference in l_c between a non-integer layered stem and integer layered crystal would be necessarily significantly smaller than for PE-48,48 or even PE-32,32. In other words, as the methylene length decreases, the formation of crystallites with esters at the surfaces is favored and any non-integer layered structures will quickly, or instantaneously, rearrange into the integer one. This explains why the shorter spaced LSAPEs do not show the minimum and why the minimum in shorter *n*-alkanes is so shallow.

While lack of any rate minima in PE-12,12 is explained above as a favored formation of integer crystals at any T_c, the observed non-integer crystal thicknesses in Fig. 8 (b) for this polyester deserves some discussion. As they are kinetically favored, the initial formation of non-integer crystals cannot be discarded. However, these metastable crystals will quickly thin or thicken toward the stable integer ones. With an expected small difference in energy barriers between the non-integer and either thinner or thicker integer forms, it is likely that at most T_c a mixture of integer crystals with 8, 9, or 10 monomer repeats are formed. Hence, even if most crystallites are of the integer type, the average crystal thickness will be a fractional number of monomer repeats.

Finally, we emphasize that this work demonstrates that the self-poisoning feature in high molecular weight polymers is not unique to systems that display thermally induced polymorphism and drastic conformational differences between various crystal types. Instead, while self-poisoning may be ubiquitous to all semi-crystalline polymers, the experimental observation of a minimum in the crystallization rate is specific to polymer systems with (at least) two energetically different crystalline structures having sufficiently different nucleation and growth kinetics. In the case studied here, the non-integer and integer layered crystals are energetically different due to a low nucleation barrier of the former with a non-integer thickness, and the thermodynamic stability afforded to the integer layered crystals by staggering the ester groups at the basal surfaces.

4. Conclusions

In this work, we have investigated in detail the isothermal crystallization kinetics and crystalline structures of four LSAPEs, PE-48,48, PE-32,32, PE-18,18, and PE-12,12. A large range of isothermal crystallization temperatures was analyzed from data obtained by conventional DSC and by Fast Scanning Calorimetry. With increasing crystallization temperature (T_c), the three longest-spaced polymers, PE-48,48, PE-32,32, and PE-18,18 form crystals with either a non-integer or integer number of ester-ester layers in the same crystallographic form. Metastable, non-integer layered crystals form in a lower T_c range and are kinetically favored, while the integer layered crystals are more thermodynamically stable and form in a higher T_c range. The transition between non-integer and integer layered crystals was identified by SAXS and is accompanied by an increase in melting temperature.

At the transition between the non-integer and integer layered crystals, anomalous rate minima in the overall crystallization rate and isothermal linear growth rate with decreasing undercooling are observed in the longest spaced polyesters. The rate minima become shallower with decreasing methylene spacer and vanish in the shortest symmetric LSAPE studied, PE-12,12. The observed rate minima are not associated with a change in the mechanism of nucleation and growth of these systems or with a transition between different polymorphs but rather with a transition between quantized crystal thicknesses. The minima are explained on the basis of self-poisoning, similarly to the rationale used to describe the effect of quantized chain folding on the crystallization rate of long-chain *n*-alkanes. At T_c approaching temperatures of the rate minima from above, depositions of metastable non-integer crystals retard growth of the integer layered crystal until the stems thicken to complete the layer placing the ester groups at the lamellar basal surfaces. The strength of this self-poisoning effect, i.e., the depth of the rate minimum, depends upon the difference in lamellar thickness between the non-integer and integer layered crystals. The latter decreases in the shortest spaced polyesters to the point that only the integer form is operative during nucleation and growth. We thus demonstrate that such an inversion in the temperature gradient of the crystallization kinetics is ubiquitous to polyethylene-like materials which form layered crystallites in at least two energetically different crystal structures.

Notes

The authors declare no competing financial interest.

CRediT authorship contribution statement

Stephanie F. Marxsen: Resources, Data curation, Formal analysis, Writing – original draft, Writing – review & editing. **Manuel Häußler:** Resources. **Marcel Eck:** Resources. **Stefan Mecking:** Resources. **Rufina G. Alamo:** Conceptualization, Project administration, Resources, Supervision, Formal analysis, Writing – original draft, Writing – review & editing, Funding acquisition.

Declaration of competing interest

The authors declare that they have no known competing financial interests or personal relationships that could have appeared to influence the work reported in this paper.

Data availability

Data will be made available on request.

Acknowledgements

Funding of this work was provided by the National Science Foundation, Polymers Program DMR- 2154026. Support of studies on degradable polyethylenes by the ERC (Advanced Grant DEEPCAT, No. 832480 to S.M.) is gratefully acknowledged. The authors thank the High Performance Materials Institute of Florida State University for access to X-ray instrumentation. The help of REU undergraduate students, Evan Curatolo and Clay Kramer with DSC and optical microscopy measurements is also acknowledged.

References

[1] F. Stempfle, P. Ortmann, S. Mecking, Long-chain aliphatic polymers to bridge the gap between semicrystalline polyolefins and traditional polycondensates, Chem. Rev. 116 (2016) 4597–4641.
[2] M. Häußler, M. Eck, D. Rothauer, S. Mecking, Closed-loop recycling of polyethylene-like materials, Nature 590 (2021) 423–427.
[3] M. Eck, S.T. Schwab, T.F. Nelson, K. Wurst, S. Iberl, D. Schleheck, C. Link, G. Battagliarin, S. Mecking, Biodegradable High-Density Polyethylene-like Material, Angew. Chemie Int. Ed. 62 (2023), e2022134.
[4] https://www.european-bioplastics.org/market/.
[5] G. Kfoury, J.-M. Raquez, F. Hassouna, J. Odent, V. Toniazzo, D. Ruch, P. Dubois, Recent advances in high performance poly(lactide): from "green" plasticization to super-tough materials via (reactive) compounding, Front. Chem. 1 (2013) 1–46. J. Jian, Z. Xiangbin, H. Xianbo, An overview on synthesis, properties and applications of poly(butylene-adipate-co-terephthalate)–PBAT, Adv. Ind. Eng. Polym. Res. 3 (2020) 19–26; Aliotta, L.; Seggiani, M.; Lazzeri, A.; Gigante, V.; Cinelli, P. A Brief Review of Poly (Butylene Succinate) (PBS) and Its Main Copolymers: Synthesis, Blends, Composites, Biodegradability, and Applications. Polymers 2022, 14, 844; K. W. Meereboer, M. Misra, A. K. Mohanty, Review of recent advances in the biodegradability of polyhydroxyalkanoate (PHA) bioplastics and their composites, Green Chem., 2020, 22, 5519–5558.
[6] L. Zhou, P. Qin, L. Wu, B.-G. Li, P. Dubois, Potentially biodegradable "short-long" type diol-diacid polyesters with superior crystallizability, tensile modulus, and water vapor barrier, ACS Sustain. Chem. Eng. 9 (2021) 17362–17370.
[7] C. Zhou, Z. Wei, Y. Yu, S. Shao, X. Leng, Y. Wang, Y. Li, Biobased long-chain aliphatic polyesters of 1,12-dodecanedioic acid with a variety of diols: odd-even effect and mechanical properties, Mater. Today Commun. 19 (2019) 450–458.
[8] G. Barbiroli, C. Lorenzetti, C. Berti, M. Fiorini, P. Manaresi, Polyethylene like polymers. Aliphatic polyesters of dodecanedioic acid, Eur. Polym. J. 39 (2003) 655–661.
[9] I. Cho, K. Lee, Poly(triacontamethylene triacontanedioate) as polyethylene analogue: properties and enzymatic degradation, Macromol. Chem. Phys. 198 (1997) 861–869.
[10] D. Quinzler, S. Mecking, Linear semicrystalline polyesters from fatty acids by complete feedstock molecule utilization, Angew. Chemie Int. Ed. 49 (2010) 4306–4308.
[11] T. Witt, M. Häußler, S. Kulpa, S. Mecking, Chain multiplication of fatty acids to precise telechelic polyethylene, Angew. Chemie Int. Ed. 56 (2017) 7589–7594.
[12] K.J. Ihn, E.S. Yoo, S.S. Im, K.J. Ihn, Structure and morphology of poly (tetramethylene succinate) crystals, Macromolecules 28 (1995) 2460–2464.
[13] P.A. Klonos, L. Papadopoulos, M. Kasimatis, H. Iatrou, A. Kyritsis, D.N. Bikiaris, Synthesis, crystallization, structure memory effects, and molecular dynamics of biobased and renewable poly(n -alkylene succinate)s with n from 2 to 10, Macromolecules 54 (2021) 1106–1119.
[14] M. Soccio, N. Lotti, L. Finelli, M. Gazzano, A. Munari, Aliphatic poly(propylene dicarboxylate)s: effect of chain length on thermal properties and crystallization kinetics, Polymer 48 (2007) 3125–3136.
[15] S. Shao, Z. Wei, Y. Wang, Y. Yu, C. Zhou, X. Leng, Y. Li, Biobased odd–odd poly (propylene dicarboxylate)s, J. Therm. Anal. Calorim. 140 (2020) 199–211.
[16] S. Qiu, Z. Qiu, Crystallization kinetics and morphology of poly(ethylene suberate), J. Appl. Polym. Sci. 133 (2016), 43086.
[17] G.Z. Papageorgioua, D.N. Bikiaris, D.S. Achiliasa, E. Papastergiadisb, A. Docoslisc, Crystallization and biodegradation of poly(butylene azelate): comparison with poly (ethylene azelate) and poly(propylene azelate), Thermochim. Acta 515 (2011) 13–23.
[18] G.Z. Papageorgiou, D.S. Achilias, D.N. Bikiaris, Crystallization kinetics and melting behaviour of the novel biodegradable polyesters poly(propylene azelate) and poly (propylene sebacate), Macromol. Chem. Phys. 210 (2009) 90–107.
[19] G.Z. Papageorgiou, D.N. Bikiaris, D.S. Achilias, N. Karagiannidis, Synthesis, crystallization, and enzymatic degradation of the biodegradable polyester poly (ethylene azelate), Macromol. Chem. Phys. 211 (2010) 2585–2595.
[20] L. Franco, J. Puiggalı, Crystallization kinetics of poly(hexamethylene succinate), Eur. Polym. J. 39 (2003) 1575–1583.
[21] Z. Qiu, T. Ikehara, T. Nishi, Crystallization behaviour of biodegradable poly (ethylene succinate) from the amorphous state, Polymer 44 (2003) 5429–5437.
[22] G.Z. Papageorgiou, D.N. Bikiaris, Crystallization and melting behavior of three biodegradable poly(alkylene succinates). A comparative study, Polymer 46 (2005) 12081–12092.
[23] C. Berti, A. Celli, P. Marchese, E. Marianucci, G. Barbiroli, F. Di Credico, The effect of aliphatic chain length on thermal properties of poly(alkylene dicarboxylate)s, E-Polymers 7 (2007).
[24] S. Gestí, A. Almontassir, M.T. Casas, J. Puiggalí, Crystalline structure of poly (hexamethylene adipate). Study on the morphology and the enzymatic degradation of single crystals, Biomacromolecules 7 (2006) 799–808.
[25] S. Gestí, M.T. Casas, J. Puiggali, Single crystal morphology and structural data of a series of polyesters derived from 1,8-octanediol, Eur. Polym. J. 44 (2008) 2295–2307.
[26] K. Nomura, N.W. Binti Awang, Synthesis of bio-based aliphatic polyesters from plant oils by efficient molecular catalysis: a selected survey from recent reports, ACS Sustain. Chem. Eng. 9 (2021) 5486–5505.
[27] M.G. Broadhurst, An analysis of the solid phase behavior of the normal paraffins, J. Res. Natl. Bur. Stand. Sect. A Phys. Chem. 66A (1962) 241.
[28] K. Yang, Z. Cai, A. Jaiswal, M. Tyagi, J.S. Moore, Y. Zhang, Dynamic odd-even effect in liquid n -alkanes near their melting points, Angew. Chemie Int. Ed. 55 (2016), 14090, 14095.
[29] W. Bin Liau, R.H. Boyd, Structure and packing in crystalline aliphatic polyesters, Macromolecules 23 (1990) 1531–1539.
[30] E. Kim, H. Uyama, Y. Doi, C.-S. Ha, T. Iwata, Crystal structure and morphology of poly(11-undecalactone) solution-grown single crystals, Macromolecules 37 (2004) 7258–7264.
[31] C.S. Fuller, C.J. Frosch, X-ray investigation of the decamethylene series of polyesters, J. Am. Chem. Soc. 61 (1939) 2575–2580.
[32] T. Kanamoto, K. Tanaka, H. Nagai, Growth and morphology of single crystals of linear aliphatic polyesters, J. Polym. Sci. 2 Polym. Phys. 9 (1971) 2043–2060.
[33] A.S. Ueda, Y. Chatani, H. Tadokoro, Structural studies of polyesters. IV. Molecular and crystal structures of poly(ethylene succinate) and poly(ethylene oxalate), Polym. J. 2 (1971) 387–397.
[34] P.A. Aylwin, R.H. Boyd, Aliphatic polyesters as models for relaxation processes in crystalline polymers: 1. Characterization, Polymer 25 (1984) 323–329.
[35] R. Chandra, R. Rustgi, Biodegradable polymers, Prog. Polym. Sci. 23 (1998) 1273–1335.
[36] I. van der Meulen, M. de Geus, H. Antheunis, R. Deumens, E.A.J. Joosten, C. E. Koning, A. Heise, Polymers from functional macrolactones as potential biomaterials: enzymatic ring opening polymerization, biodegradation, and biocompatibility, Biomacromolecules 9 (2008) 3404–3410.
[37] P. Skoglund, Å. Fransson, Crystallization kinetics of polytridecanolactone and polypentadecanolactone, Polymer 39 (1998) 3143–3146.
[38] J. Cai, B.S. Hsiao, R.A. Gross, Polypentadecalactone prepared by lipase catalysis: crystallization kinetics and morphology, Polym. Int. 58 (2009) 944–953.
[39] A. Díaz, L. Franco, J. Puiggalí, Study on the crystallization of poly(alkylene dicarboxylate)s derived from 1,9-nonanediol and mixtures with different ratios of azelaic acid and pimelic acid units, J. Polym. Res. 23 (2016) 12.
[40] S.F. Marxsen, D. Song, X. Zhang, I. Flores, J. Fernández, J.R. Sarasua, A.J. Müller, R.G. Alamo, Crystallization rate minima of poly(ethylene brassylate) at temperatures transitioning between quantized crystal thicknesses, Macromolecules 55 (2022) 3958–3973.
[41] G. Ungar, A. Keller, Inversion of the temperature dependence of crystallization rates due to onset of chain folding, Polymer 28 (1987) 1899–1907.
[42] S.J. Organ, G. Ungar, A. Keller, Rate minimum in solution crystallization of long paraffins, Macromolecules 22 (1989) 1995–2000.
[43] G. Ungar, E.G.R. Putra, D.S.M. de Silva, M.A. Shcherbina, A.J. Waddon, The Effect of Self-Poisoning on Crystal Morphology and Growth Rates, Adv Polym Sci, 2005, pp. 45–87.
[44] S.Z.D. Cheng, J. Chen, Nonintegral and integral folding crystal growth in low-molecular mass poly (ethylene oxide) fractions. III. Linear crystal growth rates and crystal morphology, J. Polym. Sci., Part B: Polym. Phys. 29 (1991) 311–327.
[45] S.F. Marxsen, M. Huβler, S. Mecking, R.G. Alamo, Isothermal step thickening in a long-spaced aliphatic polyester, Polymer 191 (2020), 122282.
[46] P. Kaner, C. Ruiz-Orta, E. Boz, K.B. Wagener, M. Tasaki, K. Tashiro, R.G. Alamo, Kinetic control of chlorine packing in crystals of a precisely substituted polyethylene. Toward advanced polyolefin materials, Macromolecules 47 (2014) 236–245.
[47] X. Zhang, W. Zhang, K.B. Wagener, E. Boz, R.G. Alamo, Effect of self-poisoning on crystallization kinetics of dimorphic precision polyethylenes with bromine, Macromolecules 51 (2018) 1386–1397.

[48] X. Zhang, X. Zuo, P. Ortmann, S. Mecking, R.G. Alamo, Crystallization of long-spaced precision polyacetals I: melting and recrystallization of rapidly formed crystallites, Macromolecules 52 (2019) 4934–4948.
[49] X. Zhang, S.F. Marxsen, P. Ortmann, S. Mecking, R.G. Alamo, Crystallization of long-spaced precision polyacetals II: effect of polymorphism on isothermal crystallization kinetics, Macromolecules 53 (2020) 7899–7913.
[50] S.F. Marxsen, M. Häußler, S. Mecking, R.G. Alamo, Crystallization of long-spaced precision polyacetals III: polymorphism and crystallization kinetics of even polyacetals spaced by 6 to 26 methylenes, Polymers 13 (2021) 1560.
[51] S.F. Marxsen, M. Häußler, S. Mecking, R.G. Alamo, Unlayered–layered crystal transition in recyclable long-spaced aliphatic polyesters, ACS Appl. Polym. Mater. 3 (2021) 5243–5256.
[52] G. Snyder, J.H. Schachtschneider, Vibrational analysis of the n-paraffins—I, Spectrochim. Acta 19 (1963) 85–116.
[53] C.G. Vonk, G. Kortleve, X-ray small-angle scattering of bulk polyethylene, Kolloid-Zeitschrift Zeitschrift Für Polym. 220 (1967) 19–24.
[54] C.G. Vonk, A.P. Pijpers, An x-ray diffraction study of nonlinear polyethylene. I. Room-temperature observations, J. Polym. Sci., Polym. Phys. Ed. 23 (1985) 2517–2537.
[55] B. Goderis, H. Reynaers, M.H.J. Koch, V.B.F. Mathot, Use of SAXS and linear correlation functions for the determination of the crystallinity and morphology of semi-crystalline polymers. Application to linear polyethylene, J. Polym. Sci., Part B: Polym. Phys. 37 (1999) 1715–1738.
[56] H. Abe, Y. Kikkawa, Y. Inoue, Y. Doi, Morphological and kinetic analyses of regime transition for poly[(S)-lactide] crystal growth, Biomacromolecules 2 (2001) 1007–1014.
[57] H. Tsuji, Y. Tezuka, S.K. Saha, M. Suzuki, S. Itsuno, Spherulite growth of l-lactide copolymers: effects of tacticity and comonomers, Polymer 46 (2005) 4917–4927.
[58] M. Yasuniwa, S. Tsubakihara, K. Iura, Y. Ono, Y. Dan, K. Takahashi, Crystallization behavior of poly(l-lactic acid), Polymer 47 (2006) 7554–7563.
[59] B. Zhu, Y. He, N. Asakawa, N. Yoshie, H. Nishida, Y. Inoue, Polymorphic crystallization and Melting Recrystallization behavior of poly(3-hydroxypropionate), Macromolecules 38 (2005) 6455–6465.
[60] J. Liu, H.-M. Ye, J. Xu, B.-H. Guo, Formation of ring-banded spherulites of α and β modifications in Poly(butylene adipate), Polymer 52 (2011) 4619–4630.
[61] F. De Santis, S. Adamovsky, G. Titomanlio, C. Schick, Isothermal nanocalorimetry of isotactic polypropylene, Macromolecules 40 (2007) 9026–9031.
[62] A. Toda, R. Androsch, C. Schick, Insights into polymer crystallization and melting from fast scanning chip calorimetry, Polymer 91 (2016) 239–263.
[63] R. Zhang, E. Zhuravlev, J.W.P. Schmelzer, R. Androsch, C. Schick, Steady-state crystal nucleation rate of polyamide 66 by combining atomic force microscopy and fast-scanning chip calorimetry, Macromolecules 53 (2020) 5560–5571.
[64] A. Toda, Y. Furushima, C. Schick, Vitrification of the entire amorphous phase during crystallization of poly(butylene terephthalate) near the glass-transition temperature, Macromolecules 56 (2023) 3110–3118.
[65] J.E.K. Schawe, Comments on isothermal crystallization kinetics of polymers: polypropylene at high supercooling, Thermochim. Acta 718 (2022), 179370.